Symmetry-Related Transitions in the Photoluminescence and Cathodoluminescence Spectra of Nanosized Cubic Y$_2$O$_3$:Tb^{3+}

Daniel den Engelsen, Paul G. Harris, Terry G. Ireland,[z] George Fern, and Jack Silver

Centre for Phosphor and Display Materials, Wolfson Centre for Materials Processing, Brunel University London, Uxbridge, Middlesex UB8 3PH, United Kingdom

Herein the photoluminescence spectra of nanosized cubic Y$_2$O$_3$:Tb^{3+} having Tb^{3+} concentrations varying between 0.1 and 10 Mol% are described. Low temperature cathodoluminescence spectra from these materials recorded in a scanning transmission electron microscope are presented and discussed. By studying the photoluminescence-spectra recorded at room temperature and focused on the $^5D_4 \rightarrow {}^7F_5$ (C$_2$) and $^5D_4 \rightarrow {}^7F_5$ (C$_{3i}$) transitions, at 542.8 and 544.4 nm respectively, it was found that the critical distance for energy transfer from Tb^{3+} ions at C$_{3i}$ lattice sites to Tb^{3+} ions at C$_2$ lattice sites was 1.7 nm; at distances >1.7 nm, which prevail at low Tb^{3+} concentration, this energy transfer virtually stops. The gradual change of the excitation spectra upon increasing the Tb^{3+} concentration is also explained in terms of energy transfer from Tb^{3+} at C$_{3i}$ sites to Tb^{3+} at C$_2$ sites. Cathodoluminescence spectra recorded at low temperatures with the scanning transmission electron microscope provided additional evidence for this radiationless energy transfer.

Recently we published a study on the cathodoluminescence (CL) of nanosized cubic Y$_2$O$_3$:Tb^{3+} particles;[1] reference to this work will be made as Part 1. We identified a few peaks in the CL spectra that are related to Tb^{3+} at C$_{3i}$ sites in cubic Y$_2$O$_3$ (the structure is that of the mineral bixbyite). In Part 1, we have indicated the C$_{3i}$ sites by S$_6$. The vast majority of the spectral lines in the CL spectra of Y$_2$O$_3$:Tb^{3+} arise from C$_2$ type transitions. We also found evidence that the two strongest emission lines in the $^5D_4 \rightarrow {}^7F_5$ transition cluster at 542.8 nm and 544.4 nm are split when recorded at low temperature. These spectral data provided insight into the energy flow from Tb^{3+} ions at C$_{3i}$ lattice sites to Tb^{3+} ions at C$_2$ lattice sites: the critical distance between a Tb^{3+} (C$_{3i}$) donor ion and Tb^{3+} (C$_2$) acceptor ion was found to be 1.7 nm, which is about 5 times larger than the shortest distance between a cation at a C$_{3i}$ site and a cation at a C$_2$ site.[1,2] It is the objective of the work described herein to gain more insight into the studies reported in Part 1 by measuring the photoluminescence (PL) spectra at room temperature and the CL spectra in a scanning transmission electron microscope (STEM) at low temperatures.

Many authors have reported on the PL spectrum of Y$_2$O$_3$:Tb^{3+}; here we shall mention only the most relevant publications on the spectroscopic characteristics of Y$_2$O$_3$:Tb^{3+}. An important result in Part 1 was the doublet structure of the 542 nm and 544 nm lines, which became noticeable at a temperature of 103 K. A similar result was reported by Song and Wang,[3] who also found 4 lines between 541 and 545 nm at 83 K. At 274 K these lines coalesced into two peaks, in which the 542 nm peak still showed a shoulder. Najafov et al.[4] showed the doublet structure of the 542 nm and 544 nm lines in the PL spectra of Y$_2$O$_3$:Tb^{3+} with various Tb^{3+} concentrations at room temperature. In the spectrum presented in their paper (Figure 5a) it can be observed that the height of the 544 nm doublet decreases with respect to the height of the 542 nm doublet upon increasing the Tb^{3+} concentration. Najafov et al. did not refer to these phenomena in their paper.[4]

Concentration quenching was identified as an important issue in several publications on the PL spectrum of Y$_2$O$_3$:Tb^{3+}. It was discussed by Najafov et al.[4] and measured by Muenchausen et al.;[5] these latter authors found that the PL efficiency peaked at 0.5 Mol% in bulk Y$_2$O$_3$:Tb^{3+} material, whereas for their nano-material with particle size of 35 nm it peaked at 1.5% Tb^{3+}. Wang et al.[6] found that the $^5D_4 \rightarrow {}^7F_5$ PL transition intensity reached a maximum value at 5.02 Mol% Tb^{3+} in electrodeposited thin films of Y$_2$O$_3$. The particle size of the crystallites in their films was not indicated. In the case of

CL, concentration quenching started at lower Tb^{3+} concentration; we found that the CL lumen efficacy of 1% Y$_2$O$_3$:Tb^{3+} is higher than that of 3% Y$_2$O$_3$:Tb^{3+}.[1] Obviously, the results of Muenchausen et al.[5] and Wang et al.[6] are contradictory; therefore, we cannot draw conclusions on possible differences between concentration quenching of Y$_2$O$_3$:Tb^{3+} in PL and in CL.

The excitation spectra of Y$_2$O$_3$:RE^{3+} (RE^{3+} being a trivalent rare earth ion) were presented by Kano in the Phosphor Handbook.[7] The excitation band of Y$_2$O$_3$:Tb^{3+} represented in Kano's chapter shows two peaks, one at 304 nm and the other at 280 nm; however, it is not indicated which transitions were used to monitor these excitation spectra. Other reports on the excitation spectrum of Y$_2$O$_3$:Tb^{3+} were given by Ropp,[8] Najafov et al.,[4] Muenchausen et al.,[5] Meng et al.,[9] Liu et al.,[10] Ray et al.,[11] Loitongbam et al.[12] and Som et al.[13] Most authors assigned the broad excitation band between 260 nm and 310 nm to a 4f^8$\rightarrow$4f^{7}5d^1 transition in the Tb^{3+} ion. Only Ray et al.[11] and Loitongbam et al.[12] designated this excitation band as a charge transfer (CT) band. A third possibility, direct Tb^{3+} excitation through a 4f^8$\rightarrow$4f^8 transition, was mentioned by Som et al.[13] We shall adopt here the assignment of Kano:[7] the excitation band between 260 nm and 340 nm is due to 4f^8$\rightarrow$4f^{7}5d^1 transitions, since the CT band of Y$_2$O$_3$:Tb^{3+} is positioned at 64000 cm^{-1} (156 nm) in the VUV. These assignments were confirmed by Dorenbos, see for instance Ref. 14 and publications cited in this recent paper. No attention was paid in the papers[3–6,8–13] to symmetry-related transitions and effects in the spectrum of Y$_2$O$_3$:Tb^{3+}, mainly because the lines at 542 nm and 544 nm in the emission PL spectra were not observed as split (due to poor resolution of the spectrometers) or their behavior was overlooked and thus, not taken into consideration. Laser-excited spectra of photonic bandgap Y$_2$O$_3$:Tb^{3+} material were reported by Withnall et al.[15] in a temperature range from 25–400°C. These temperatures were too high to split the Y$_2$O$_3$:Tb^{3+} $^5D_4 \rightarrow {}^7F_5$ doublets at 542 nm and 544 nm.

Materials and Methods

The synthesis of nanosized cubic Y$_2$O$_3$:Tb^{3+} particles (in-house) has been described in detail in Part 1. Figure 1 shows panchromatic STEM images of the CL emitted by 0.1% Y$_2$O$_3$:Tb^{3+} at −171.3° C and beam energy of 200 keV and 10% Y$_2$O$_3$:Tb^{3+} at room temperature and 80 keV. The particle size varied from 130 to 200 nm in the 0.1% sample, but was much smaller in the 10% sample. It can be seen that the particles consist of smaller crystallites, which have dimensions of about 40 nm. In Part 1, we presented images of Y$_2$O$_3$:Tb^{3+} particles at other Tb^{3+} concentration.

[z]E-mail: terry.ireland@brunel.ac.uk
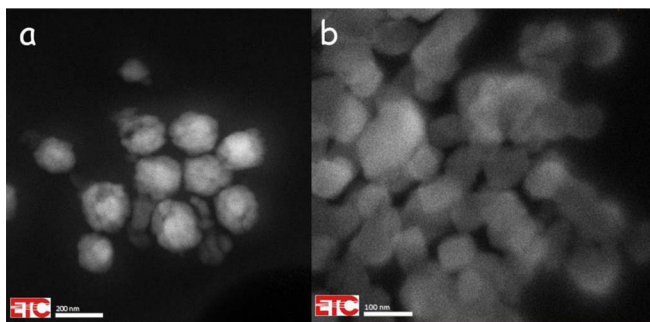
Figure 1. Panchromatic images of $Y_2O_3:Tb^{3+}$ recorded with Vulcan detector of STEM. a: $0.1\%Y_2O_3:Tb^{3+}$ at $-171°C$ and 200 keV. b: 10% $Y_2O_3:Tb^{3+}$ at room temperature and 80 keV.

PL emission spectra of the $Y_2O_3:Tb^{3+}$ samples were measured with a Bentham phosphor spectrometer system (Bentham Instruments Ltd., Reading, UK), configured with M300 excitation and emission monochromators and equipped with 0.37 mm slits. The resolution of the spectrometer was insufficient to detect the doublet structure of the strong emission lines at 542.5 and 544.2 nm.[1] The absolute wavelength calibration of this emission monochromator could be off by maximally 0.4 nm; however, relative wavelength values were accurate within 0.3 nm. All PL spectra were recorded at room temperature. The minimum wavelength in the excitation spectra was 250 nm.

Figures 1a and 1b are panchromatic CL images recorded with a STEM, model 2100F, JEOL, Japan, equipped with a Vulcan CL detector, Gatan, USA, for imaging and spectroscopic purposes. Details of this equipment were also described in Part 1.

Results

Figure 2 is an overlay of two PL spectra of 1% $Y_2O_3:Tb^{3+}$ between 460 and 700 nm: one excited at 282 nm and the other excited at 305 nm. The $^5D_4\rightarrow^7F_J$ (J = 1, 2... 6) transition clusters are indicated in Figure 2. The weak emission lines of the $^5D_4\rightarrow^7F_2$ transition cluster are noticeable at ∼666 nm, even the weaker lines of the $^5D_4\rightarrow^7F_1$ transition cluster at ∼688 nm can be observed. The spectra excited at 282 nm and 305 nm are different, although not so noticeable in Figure 2. In the next figures the relevant differences will be magnified. Exciting cubic $Y_2O_3:Tb^{3+}$ with radiation between 260 nm and 285 nm wavelength results in mainly C_2 type emission lines, whereas excitation at 305 nm results in the C_{3i} type emission lines becoming more visible. This can be seen in Figure 3 for the $^5D_4\rightarrow^7F_5$ transition cluster. This symmetry-related assignment is based on the analyses of the CL spectra reported in Part 1: the peak at 542.5 nm was identified as C_2 and the peak at 544.2 nm as C_{3i}. The spectra in Figure 3
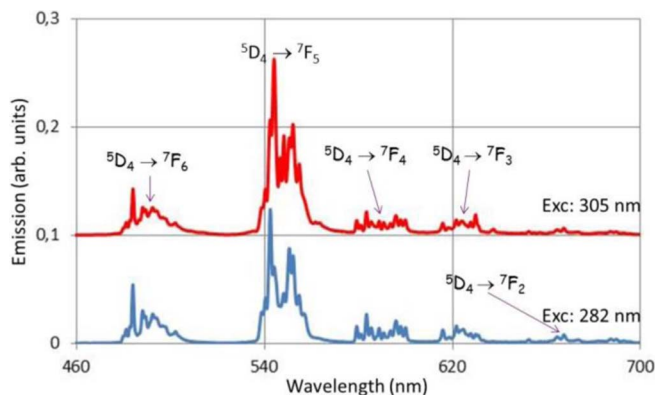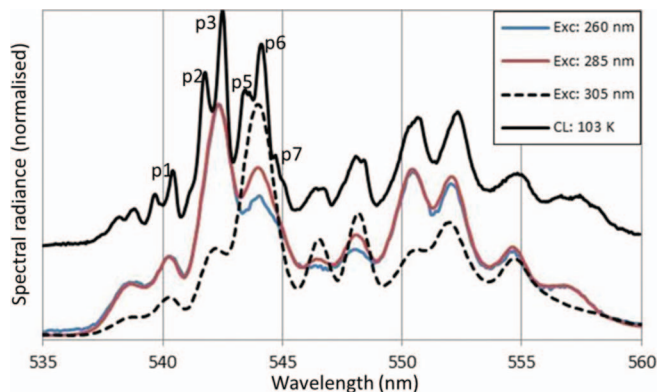

Figure 3. Overlay of PL spectra of $^5D_4\rightarrow^7F_5$ transition cluster of 0.3% $Y_2O_3:Tb^{3+}$ excited at 260 nm, 285 nm and 305 nm. The CL spectrum of 0.7% $Y_2O_3:Tb^{3+}$ was recorded in the TEM at beam energy of 80 keV and temperature of 103 K. The peaks between 540 nm and 545 nm in the CL spectrum have been labeled for deconvolution purposes.

have been normalized to the highest peak in each spectrum to enhance the visibility of the differences. Exciting 0.3% $Y_2O_3:Tb^{3+}$ between 260 nm and 285 nm enhances the peak at 542.5 nm rather than the peak at 544.2 nm, whereas excitation at 305 nm reverses the outcome. The CL spectrum recorded at low temperature shows that the peaks at 542.5 nm and 544.2 nm are doublets.

Excitation spectra of $Y_2O_3:Tb^{3+}$ monitored at various emission peaks are represented in Figure 4. The spectra shown in Figures 4a and 4b are quite different at low Tb^{3+} concentrations, whilst at high Tb^{3+} concentration they show a tendency to become more equal. In Figure 4a the maximum is at about 282 nm, while Figure 4b shows a maximum at 305 nm. The excitation spectrum of 10% $Y_2O_3:Tb^{3+}$ manifests a small absorption band at 338 nm, which is not noticeable in the spectra of the other $Y_2O_3:Tb^{3+}$ samples. The excitation spectrum of $Y_2O_3:Tb^{3+}$ has weaker bands in the range 340 nm < λ < 500 nm (where λ is wavelength), as illustrated in Figures 4c and 4d. In Figure 4c a tentative assignment of some bands has been indicated. There seems to be no symmetry-related effect in Figure 4c. Figure 4d shows the excitation spectra when monitoring at the 629.8 nm and 621.5 nm peaks of the $^5D_4\rightarrow^7F_3$ transition cluster. These peaks have been assigned as C_{3i} and C_2 type transitions respectively in Part 1, and their behavior in PL spectra will be shown hereafter. Between 460 nm < λ < 500 nm, the bands of the top and bottom spectra in Figure 4d appear at the same wavelength, between 380 nm < λ < 460 nm the peaks of the top spectrum have got a blueshift with respect to those in the bottom spectrum. Although we did not assign the transitions of those peaks, we assume that corresponding bands belong to the same transitions and that the shift between the upper and lower spectrum is caused by Tb^{3+} located at C_{3i} sites (bottom) and Tb^{3+} located at C_2 sites (top).

The excitation spectra represented in Figures 4a and 4b can be deconvoluted with two Gaussian profiles, E1 and E2, as shown in Figures 5a and 5b. The algorithm for a Gaussian-type deconvolution has been described in Part 1 and will not be repeated here. The Gaussian profiles were fitted to the experimental spectra with a least squares algorithm. Lorentzian profiles did not yield a satisfactory fit, because these profiles are too broad at low values of the spectral absorption and yielded least squares sums that were about 100 times larger than those for the Gaussian profiles. The E1-peak is broader than the E2 peak. Najafov et al.[4] and Som et al.[12] also made a Gaussian deconvolution of the excitation band for $Y_2O_3:Tb^{3+}$ between 250 nm and 340 nm. They also found that the E2 peak was narrower than the E1-peak. Som et al.[12] estimated the full width at half maximum (FWHM) of E1 and E2 at 0.45 eV and 0.26 eV respectively. These values are smaller than our results, which are 0.58 eV and 0.29 eV. In Figure 6 we have plotted the ratio between the integrated absorptions (IA) of E1 and E2, viz. IA_{E1}/IA_{E2}, as a function of the Tb^{3+} concentration.

Figure 2. PL spectra of 1% $Y_2O_3:Tb^{3+}$ excited at 282 and 305 nm.
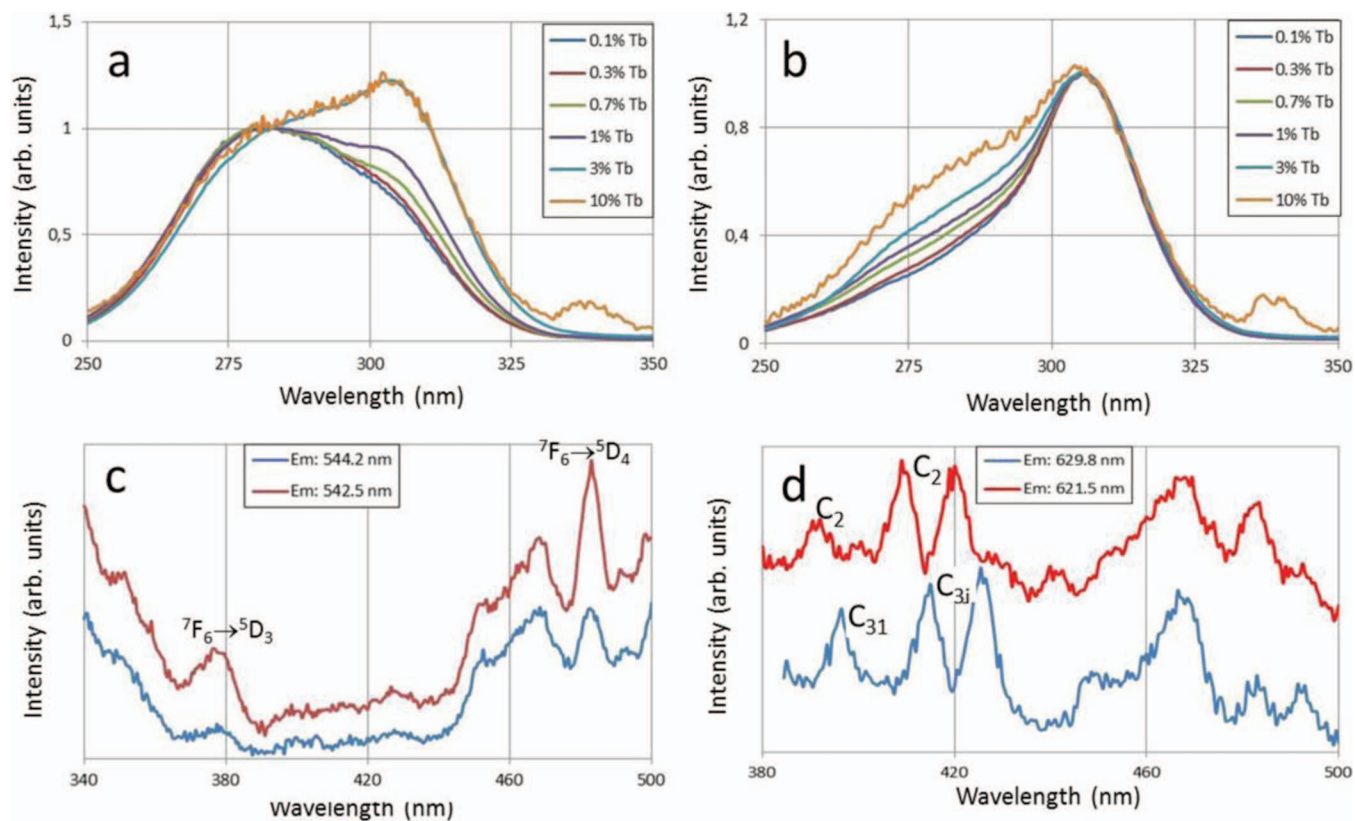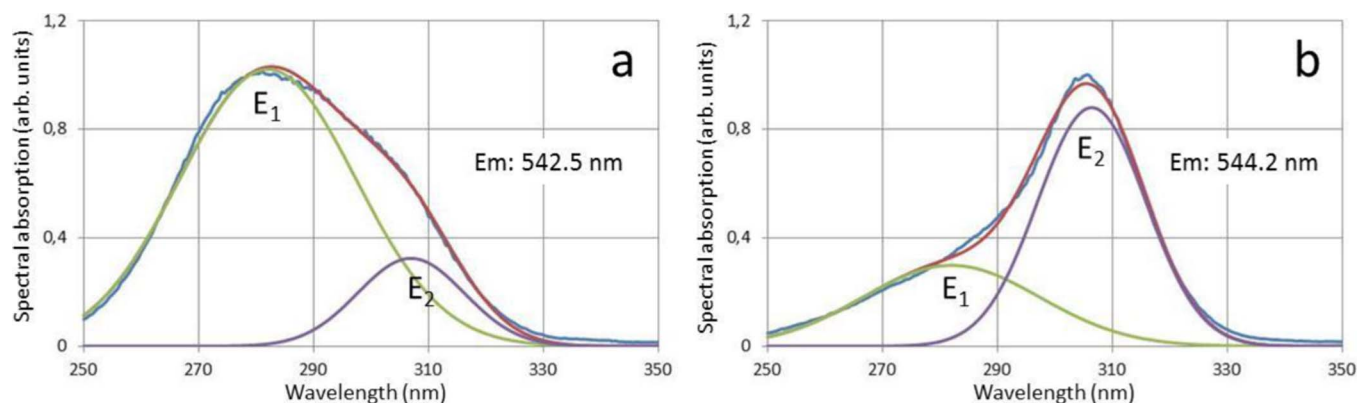
Figure 4. Excitation spectra of Y_2O_3:Tb^{3+} a: monitored at 542.5 nm. b: monitored at 544.2 nm. c: 3% Y_2O_3:Tb^{3+} between 340 and 500 nm. d: 1% Y_2O_3:Tb^{3+} between 380 and 500 nm.
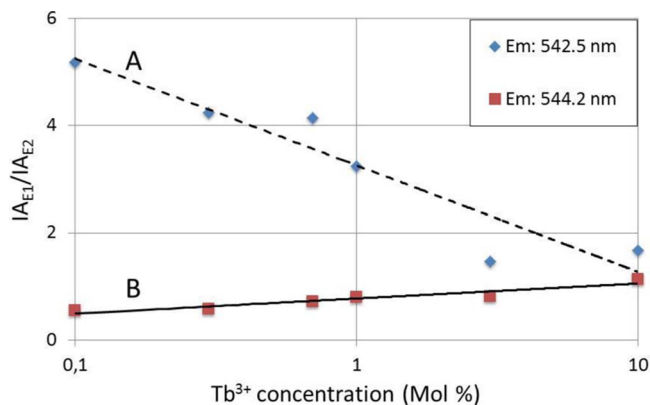
Integrated absorption refers to the area under the E1 or E2 peaks. We assign the E1 peak in Figure 5 to the $^7F_6 \rightarrow {}^9D_J$ (C_2) excitation and the E2 peak to the $^7F_6 \rightarrow {}^9D_J$ (C_{3i}) excitation, in which the ^9D_J levels have the $4f^7 5d^1$ electron configuration. This issue will be considered in more detail in the Discussion section. In the case of monitoring the emission at the C_{3i}-transition at 544.2 nm (line B) we see a slight increase of the E1-peak (C_2-type) with Tb^{3+} concentration in Figure 4b and Figure 6. Figure 4a shows an increase of C_{3i}-characteristics with Tb^{3+} concentration, which is also clearly reflected in Figure 6 by the negative slope of line A, indicating the decreasing IA_{E1}/IA_{E2} ratio monitored at 542.5 nm.

PL spectra of the $^5D_4 \rightarrow {}^7F_5$ transition cluster are depicted in Figure 7: Figure 7a shows the spectra excited at 282 nm, while Figure 7b shows the spectra excited at 305 nm. For comparison reasons these spectra are normalized: at 542.5 nm for Figure 7a and at 544.2 nm for

Figure 7b. The differences between the spectra in Figures 7a and 7b are striking: Figure 7a does not show large differences between the normalized spectra, whereas the differences in Figure 7b are large. The peak at 544.2 nm is not the only one that shows C_{3i} character, the peaks at 548.1 nm, 550.3 nm and 552 nm also show C_{3i} character, albeit less than the peak at 544.2 nm. This can be concluded from the variations shown in Figure 7b. The symmetry-related effects as shown in Figure 7 are most pronounced for the $^5D_4 \rightarrow {}^7F_5$ transition cluster, for the other transition clusters these are less. Figure 8 shows PL spectra of the $^5D_4 \rightarrow {}^7F_3$ transition cluster of Y_2O_3:Tb^{3+} between 610 nm and 640 nm, being the second transition cluster that shows clear concentration effects, which we interpret as symmetry-related effects. It can be seen that the peaks at 629.8 nm and 637 nm have C_{3i} character, because these peaks decrease with respect to the other peaks at high Tb^{3+} concentration when excited at 305 nm. A similar

Figure 5. Deconvolution of excitation spectra of 0.1% Y_2O_3:Tb^{3+}; a: C_2-type spectrum, monitored at 542.5 nm; b: C_{3i}-type spectrum, monitored at 544.2 nm.

Figure 6. Ratio of integrated absorption (IA) of peaks E1 and E2 in the excitation spectra of Y_2O_3:Tb^{3+}. Line A refers to the excitation spectra monitored at 542.5 nm, while line B refers to the excitation spectra monitored at 544.2 nm.

conclusion was drawn after analyzing the CL spectra of the $^5D_4 \rightarrow {}^7F_3$ transition cluster of Y_2O_3:Tb^{3+} in Part 1 (Figure 5c).[1] The PL spectra of the $^5D_4 \rightarrow {}^7F_6$ and $^5D_4 \rightarrow {}^7F_4$ transition clusters of Y_2O_3:Tb^{3+} do not have strong isolated C_{3i} type peaks. At room temperature the C_{3i} type peaks are overlapped by stronger C_2 type peaks in these clusters. The spectra of 10% Y_2O_3:Tb^{3+} are noisy because of concentration

quenching, which yields a low luminous efficiency. Because of the 7 to 10 times weaker emission peaks in the $^5D_4 \rightarrow {}^7F_3$ transition cluster than those in the $^5D_4 \rightarrow {}^7F_5$ transition cluster, we did not analyze the phenomena shown in Figure 8.

The analysis of the concentration effect shown in Figure 7b requires a deconvolution of the measured spectra. This deconvolution has now been done with Lorentzian profiles. Gaussian profiles have been used in Part 1, because at that time it was not clear that the 542.5 nm and 544.2 nm peaks were doublets, as shown in Figure 3. The consequence is that a better representation is obtained with Lorentzian profiles that are narrow at spectral radiances > half maximum and broad at the bottom.

The spectral radiance SR(λ), where λ represents the wavelength of a Lorentzian profile, can be written as:

$$SR(\lambda) = \sum_i \frac{A_i}{1 + \frac{(\lambda - \lambda_i)^2}{s_i^2}}, \quad [1]$$

where A_i is the maximum spectral radiance of the ith peak, λ_i is the wavelength at the maximum, s_i is the half width at half maximum and the radiance R_i of the ith transition is

$$R_i = \int_{-\infty}^{\infty} \frac{A_i d\lambda}{1 + \frac{(\lambda - \lambda_i)^2}{s_i^2}} = A_i s_i \pi. \quad [2]$$

An example of the deconvolution of the $^5D_4 \rightarrow {}^7F_5$ peaks at 542.5 nm and 544.2 nm is shown in Figure 9 for 1% Y_2O_3:Tb^{3+}. In this deconvolution seven Lorentzian profiles were used. The width parameter
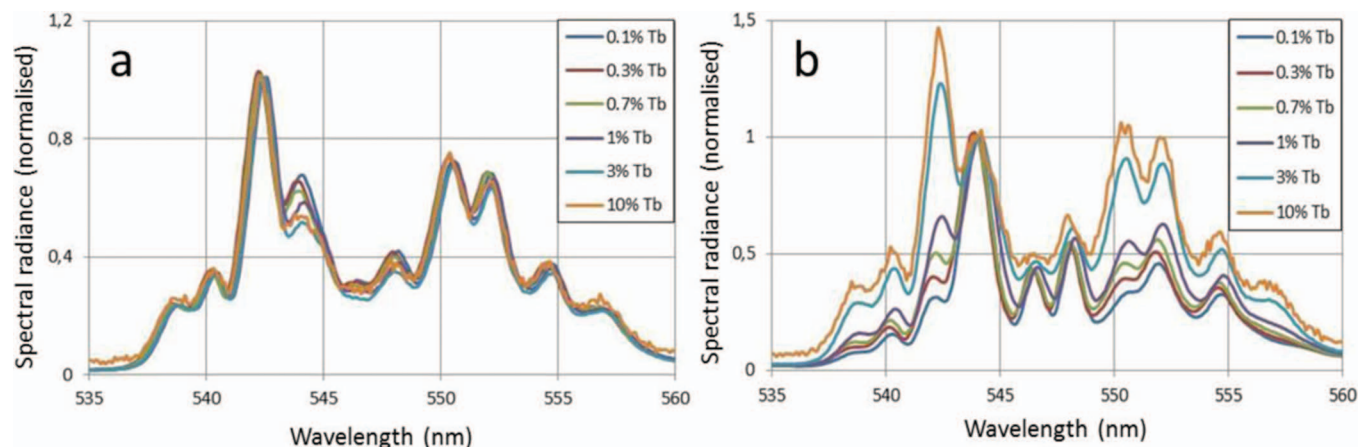
Figure 7. PL spectra of the $^5D_4 \rightarrow {}^7F_5$ transition cluster of Y_2O_3:Tb^{3+} at various Tb^{3+} concentrations. a: Excited at 282 nm and normalized at 542.5 nm. b: Excited at 305 nm and normalized at 544.2 nm.
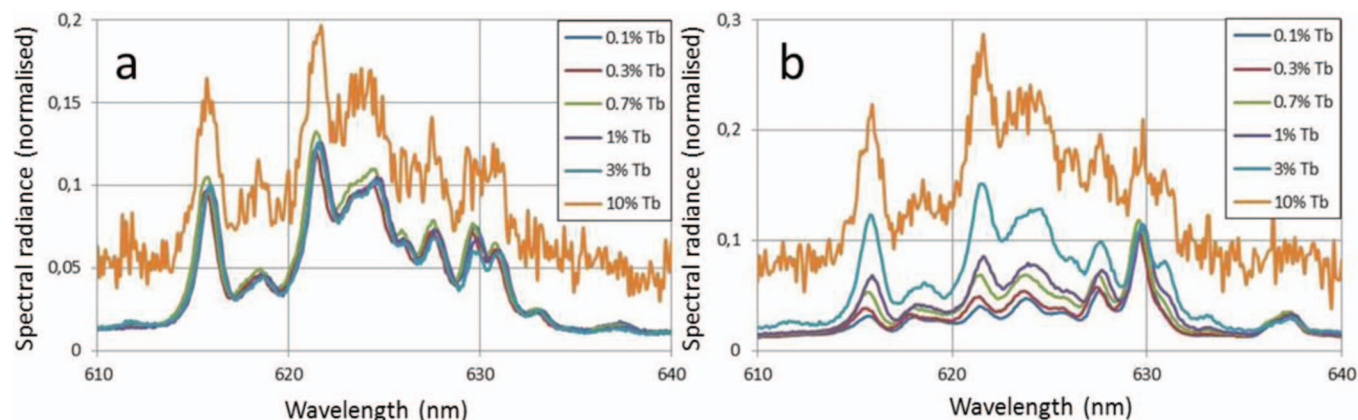
Figure 8. PL spectra of the $^5D_4 \rightarrow {}^7F_3$ cluster of Y_2O_3:Tb^{3+} at various Tb^{3+} concentrations. a: Excited at 282 nm and normalized at 542.5 nm. b: Excited at 305 nm and normalized at 544.2 nm.
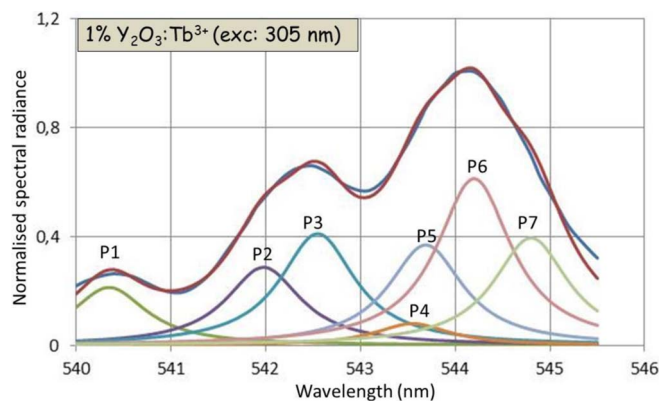
Figure 9. Deconvolution of a part of the $^5D_4 \rightarrow {}^7F_5$ spectrum between 540 and 546 nm with seven Lorentzian profiles (p1, p2, . . . p7).

Figure 10. Plot of R_{p3}/R_{p6} as a function of Tb^{3+} concentration. Curve A: PL data of Figure 7b, Line B: PL data of Figure 7a, Curve C: CL data at 200 keV and T = 103 K (Figure 11b), Curve D: CL data at 15 keV and T = 300 K (from Part 1[1]).

s_i was set equal for these seven peaks and the peak wavelengths λ_i were fitted manually. The amplitudes A_i were fitted to the measured PL spectrum with a least squares algorithm using Microsoft's Excel Solver software.

The seven Lorentzian profiles that represent the measured spectrum are indicated in Figure 9 as p1, p2,. . . p7. The most relevant are p2, p3, p5 and p6, because the radiances of these peaks are used for further analyses.

The radiance ratio R_{p3}/R_{p6} has been plotted in Figure 10 as a function of the Tb^{3+} concentration in a double log plot. Plots of R_{p2}/R_{p5} or $(R_{p2} + R_{p3})/(R_{p5} + R_{p6})$ versus Tb^{3+} concentration yield almost the same results and will not be considered here. Figure 10 summarizes the most important results of the PL and CL spectra of Y_2O_3:Tb^{3+}. Curve A is based on the PL spectra excited at 305 nm. This curve shows the largest variation of R_{p3}/R_{p6} versus Tb^{3+} concentration. Line B is based on the PL spectra excited at 282 nm and shows a limited variation. Curve C in Figure 10 is based on the CL spectra recorded with the spectrometer connected to the TEM at 200 keV and $-170°C$ as shown in Figure 11b; this will be discussed in the next paragraphs. Curve D, copied from Part 1, is based on the CL-spectra recorded at 15 keV at room temperature. Curves A, C and D show a knee at about 0.7% Tb^{3+}. In Part 1 a relation between the average distance D_{Tb} between two Tb^{3+} ions in the Y_2O_3 lattice and the Tb^{3+} concentration has been given. At 0.7 Mol % Tb^{3+} D_{Tb} is 1.7 nm, hence from the PL spectra excited at 305 nm we also find that the critical distance, $D_{Tb^{3+}}^{Crit}$, for interaction between the C_{3i} and C_2 sites is 1.7 nm. It is expected that line B does not show any concentration dependence. However, Figure 5 shows that when irradiating Y_2O_3:Tb^{3+} at 282 nm also some
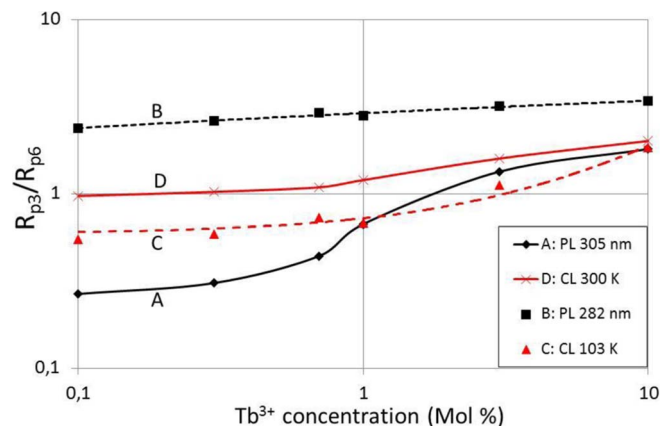
energy will be absorbed by Tb^{3+} at C_{3i}-sites (E2-band). This explains why line B is not flat.

We have presented preliminary measurements of the CL spectra of 3% Y_2O_3:Tb^{3+}, which have been recorded with the Vulcan CL detector of the TEM at various temperatures in Part 1. We have now extended these measurements to other concentrations and the results are presented in Figures 11 and 12. Notwithstanding long integration times of about 500 s, the spectra of the $^5D_4 \rightarrow {}^7F_5$ transition cluster of Y_2O_3:Tb^{3+} are quite noisy. The temperatures indicated in Figure 11a refer to thermocouple readings of the sample holder. It is assumed that the temperatures of the holder and that of the phosphor particles on the C-grid are identical. We shall come back to this assumption in the Discussion section. The spectra of the $^5D_4 \rightarrow {}^7F_J$ ($J \neq 5$) transition clusters were too weak to be recorded. Figure 11a illustrates the increased splitting of the doublets centered at 542.5 nm and 544.2 nm that is observed at low temperature, presumably because of lower levels of vibronic broadening. Furthermore, the doublet peak centered at 542.2 nm increases with respect to that centered at 544 nm when the temperature is increased. Figure 11b shows a similar trend: the doublet at 542.2 nm increases, while the doublet at 544 nm decreases when the concentration of Tb^{3+} in the Y_2O_3 lattice is raised. It can be seen in Figure 11b that the 542.5 nm and 544.2 nm transitions are clearly split at $-170°C$ for all concentrations (10%Y_2O_3:Tb^{3+} has not been indicated in Figure 11b).

In order to quantify the effects depicted in Figure 11, the spectra need to be deconvoluted. This was achieved with seven Lorentzian
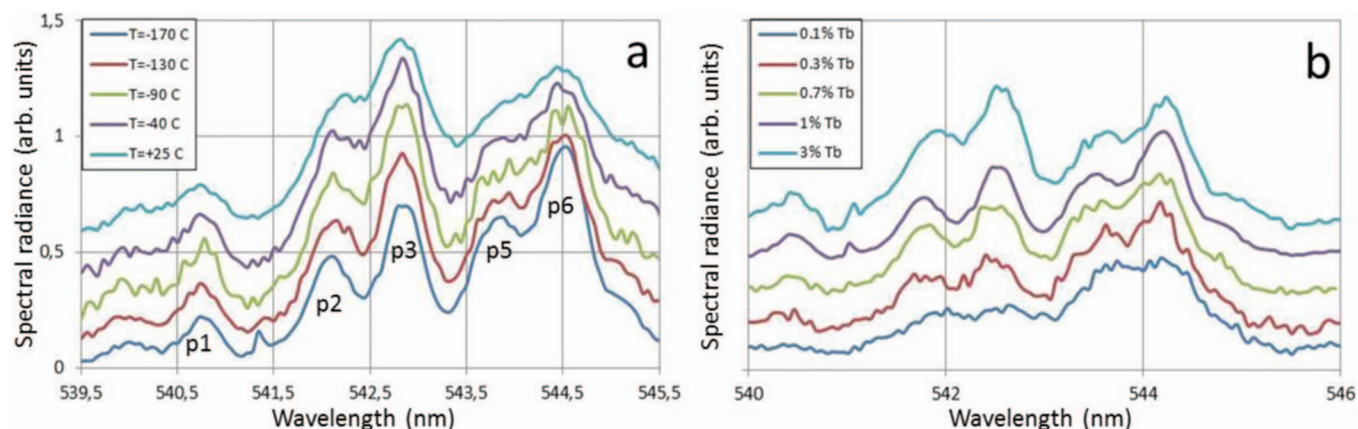
Figure 11. CL spectra of recorded at 200 keV with Vulcan CL detector. a: Spectra of 1% Y_2O_3:Tb^{3+} at various temperatures. b: Spectra at $-170°C$ and various Tb^{3+} concentrations. Spectra have been shifted vertically to improve clarity.
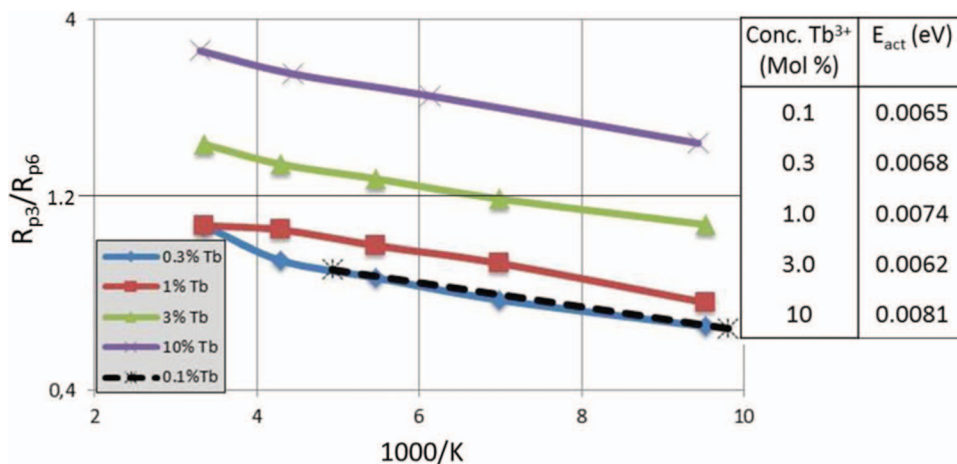
Figure 12. Arrhenius plot of R_{p3}/R_{p6}.

profiles using the same algorithm as described above. Gaussian profiles were inadequate in this case. The full width half maximum (FWHM), being $2s_i$ for a Lorentzian profile, increases almost linearly with temperature from 0.56 nm at $-170°$ C to 0.88 nm at $25°$ C for 0.3% $Y_2O_3:Tb^{3+}$. For reasons of identification the peaks in Figure 11a have been numbered in the same way as those in Figures 3 and 9. Figure 12 shows an Arrhenius plot of R_{p3}/R_{p6}, being the ratio of the radiances of the peaks p3 and p6, as indicated in Figures 9 and 11a. The activation energy for the ratio R_{p3}/R_{p6} is indicated in the table combined with Figure 12. From this table we estimate that the average activation energy is 0.007 eV.

As mentioned above, curve C in Figure 10 is based on the CL spectra depicted in Figure 11b. This curve refers to a temperature of 103 K. Although the knee is less pronounced than that in curve A, these two curves indicate the same trend and support the foregoing conclusion on the value of the critical distance, $D_{Tb^{3+}}^{Crit}$, for interaction between the C_{3i} and C_2 sites in $Y_2O_3:Tb^{3+}$. It is worth noting that the ratio R_{p3}/R_{p6} that can be derived from the CL spectrum shown in Figure 3 does not agree with the ratio for the 0.7% $Y_2O_3:Tb^{3+}$ material that has been derived from Figure 11b. The reason is that in recording the CL spectrum shown in Figure 3 the beam energy in the TEM was lowered from 200 keV to 80 keV in order to get a less noisy spectrum. In doing so, the $Y_2O_3:Tb^{3+}$ saturated: Tb^{3+} ions at C_{3i} sites were more seriously affected by saturation than Tb^{3+} ions at C_2 sites. The same phenomenon has been described in Part 1 by excitation at

5 keV and changing the current density. The trend of the CL spectra shown in Figure 11b corresponds to the sequence shown in Figure 5a of Part 1, thus, it can be concluded that the TEM spectra in Figure 11b refer to the non-saturated condition.

Discussion

First the energy transfer from Tb^{3+} at a C_{3i} lattice site to Tb^{3+} at a C_2 lattice site will be considered. For this purpose we have depicted in Figure 13 the energy levels based on the assignments for the excitation bands between 250 nm and 340 nm and the strongest emission peaks in the $^5D_4 \rightarrow {}^7F_5$ transition cluster of $Y_2O_3:Tb^{3+}$. Figure 13a is an overall picture, whereas Figure 13b zooms in on the main peaks of the $^5D_4 \rightarrow {}^7F_5$ transition cluster. In the following analysis it is assumed that excited energy levels of Tb^{3+} in the Y_2O_3 lattice are not saturated; saturation will be considered in the second half of this section. Based on the analyses of the CL spectra of $Y_2O_3:Eu^{3+}$,[2] we have assigned the 542.4 nm and 544.2 nm peaks in the spectrum of $Y_2O_3:Tb^{3+}$ as C_2 and C_{3i} respectively in Part 1. It is tempting to make the same assignment for the excitation spectrum, viz. the peaks E1 and E2 in Figure 5. In doing so, E1 would represent a C_2 excitation peak and E2 a C_{3i} peak, as mentioned before.

The crystal field splitting of the ^9D_J level for the $4f^7 5d^1$ electron configuration of Tb^{3+} in Y_2O_3 is much larger than that for the $4f^8$ configuration. This explains the broadening of the E1 and E2 peaks
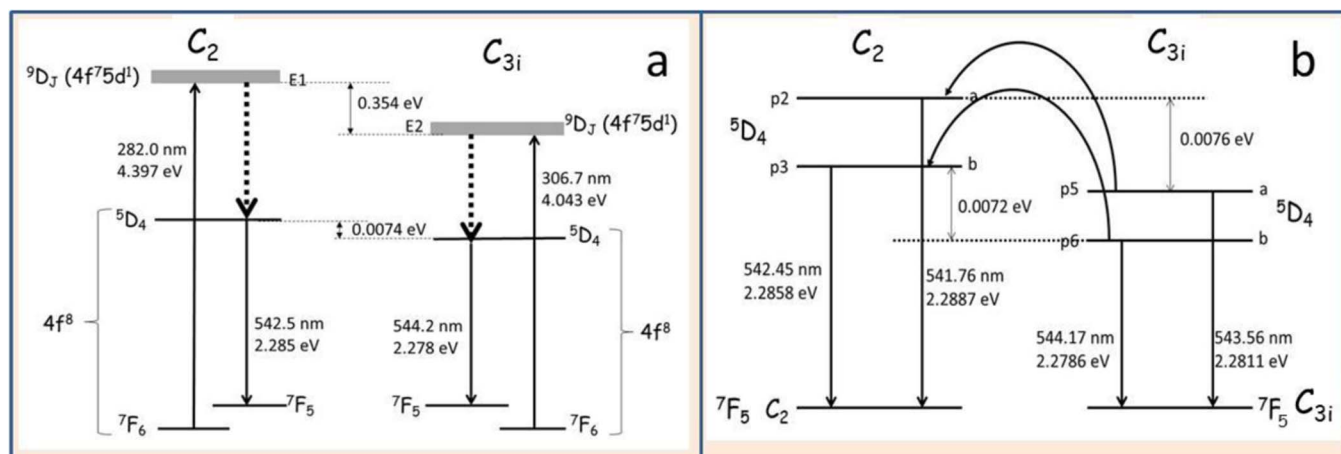
Figure 13. Energy levels involved in the excitation band and $^5D_4 \rightarrow {}^7F_5$ transition cluster of $Y_2O_3:Tb^{3+}$. a: Excitation mechanism; E1 and E2 refer to the peaks shown in Figure 5. b: Energy transfer from $^5D_4$ (C_{3i}) to $^5D_4$ (C_2). For reasons of clarity the energy scale has been distorted.

in the excitation spectra represented in Figures 4 and 5 as compared to the narrow $4f^8 \rightarrow 4f^8$ transitions shown in Figures 2 and 3. This broadening is also indicated in Figure 13a by the broad ^9D_J levels for the C_2 and C_{3i} symmetry. After excitation to one of the ^9D_J levels, energy trickles via radiationless energy loss processes down to the $^5D_4$ (C_2) or $^5D_4$ (C_{3i}) levels respectively. At sufficiently high temperatures and close distances between Tb^{3+} at C_{3i} lattice sites and Tb^{3+} at C_2 lattice sites (or high Tb^{3+} concentration), energy may be transferred as indicated in Figure 13b. This will occur between the two $^5D_4$ levels, because the energy separation is only 0.0074 eV, whereas the energy difference between the two ^9D_J levels is 0.354 eV. The Arrhenius type analysis of the radiance ratio between p3 and p6, shown in Figure 12, is a confirmation of this conclusion: the activation energy of 0.007 eV is identical to the energy difference between the $^5D_4$ (C_2) and $^5D_4$ (C_{3i}) levels indicated in Figure 13b. The energy difference between p5 and p2 is 0.0076 eV and between p6 and p3 it is 0.0072 eV, being only slightly different from the average difference indicated in Figure 13a. From the Arrhenius type analysis, we can exclude p6→p2 and p5→p3 uplifting schemes, because these have quite different energy separations.

The next issue to consider is the shape of the excitation band of cubic nanosized Y_2O_3:Tb^{3+} between 250 nm and 340 nm shown in Figure 4. Based on the variation of the height of this excitation band as a function of particle size, Meng et al.[8] concluded that this band is a $4f^8 \rightarrow 4f^75d^1$ transition. The spectra recorded by Meng et al. did not show a change of the relative heights of the constituting peaks E1 and E2 as a function of particle size. The FWHM values of the excitation peaks E1 and E2 as measured by us are 0.58 eV and 0.28 eV respectively. These values are about two orders of magnitude larger than the FWHMs of the $4f^8 \rightarrow 4f^8$ emission peaks, for example the FWHM of the p6 peak (544.4 nm) is 0.004 eV at room temperature. The FWHMs of the excitation band in Y_2O_3:Tb^{3+} resemble those of the $4f^8 \rightarrow 4f^75d^1$ transitions in BaF_2:Tb^{3+}[16] and thus, this agrees with the $4f^8 \rightarrow 4f^75d^1$ assignment suggested by Kano[7] and Dobrowolska et al.[14]

A feature that not has been reported previously is that the excitation band between 250 nm and 340 nm of Y_2O_3:Tb^{3+} shows symmetry-related effects, just like the emission peaks at 542.5 nm and 544.2 nm of the $^5D_4 \rightarrow {}^7F_5$ transition cluster. This raises the question what is the correspondence of the change of the peak ratios indicated in Figures 6 and 10. Figure 6 shows two lines, A and B, referring to different monitoring transitions. Unlike Figure 6, curves A, C and D in Figure 10 show a knee, from which the critical distance of energy flow from Tb^{3+} at a C_{3i} lattice to Tb^{3+} at a C_2 lattice site has been derived. When monitoring the excitation energy at the 542.5 nm peak (C_2) one has to realize that at high Tb^{3+} concentration a part of the energy will come from Tb^{3+} at C_{3i} lattice sites according to the mechanism shown in Figure 13b. This explains the negative slope of line A depicted in Figure 6. Line B in this graph has a positive slope. When monitoring the emission at the 544.2 nm peak (C_{3i}) we have some interference from the p3 peak at 542.5 nm (C_2) at high Tb^{3+} concentration, as shown in Figure 9. Since p3 (C_2-type) will increase with the Tb^{3+} concentration, as shown in Figure 7b, the overlap with the p5-p6 (C_{3i}-type) peak will increase as well. This explains the increase of the C_2 content (or positive slope) of line B in Figure 6, because unambiguous monitoring of C_2 or C_{3i} transitions is not possible due to interferences from overlapping peaks. This overlapping argument is irrelevant for line A, because both Figure 7a and line B in Figure 10 indicate that the heights of the 542.5 nm and 544.2 nm peaks change only slightly as a function of the Tb^{3+} concentration. Conversely, the limited variation of R_{p3}/R_{p6} (line B) in Figure 10 is an indication that energy is transferred from Tb^{3+} at C_{3i} sites to Tb^{3+} at C_2 sites and not vice versa. Curve A in Figure 10 shows a larger variation of R_{p3}/R_{p6} versus Tb^{3+} concentration than the CL-based curves C and D. This is caused by the specific excitation of Tb^{3+} at C_{3i}-sites for curve A, whereas in the case of curves C and D the Y_2O_3 lattice is excited and the energy flows to Tb^{3+} at both C_2- and C_{3i}-sites: hence, the variation of R_{p3}/R_{p6} is less.

Saturation of the 544.2 nm peak (C_{3i}) at continuous irradiation of an electron beam was discussed in Part 1 in terms of the classical theory of Bril and Kröger.[17] For reasons of completeness we shall reproduce a part of those arguments here. At high current densities j the radiance R_i of transition i can be written as

$$R_i(j) = \frac{j\eta_i}{1 + j\eta_i\tau_i/N_i}, \qquad [3]$$

where η_i is the efficiency of transition i at low current density, τ_i is the 1/e decay time of transition i and N_i is the number of Tb^{3+} ions per cm^3 at a C_2 or C_{3i} lattice site. In this analysis i = p3 or p6, because within the accuracy limit of the deconvolutions the ratios p2/p3 and p5/p6 are constant and the ratio between the radiance of the C_2 and C_{3i} type transition can well be represented by R_{p3}/R_{p6}. When at (very) large current density the second term in the denominator becomes larger than 1, then Eq. 3 can be simplified to

$$R_i = \frac{N_i}{\tau_i}. \qquad [4]$$

Eq. 4 represents the saturation limit, in which the radiance is no longer a function of the current density. There are three times more Tb^{3+} ions at C_2 sites than at C_{3i} sites, τ_{p6} = 5.8 ms and τ_{p3} = 1.7 ms at 0.7% Y_2O_3:Tb^{3+},[1] thus, the ratio R_{p3}/R_{p6} at saturation for this Tb^{3+} concentration becomes 10. In other words, the C_{3i} type transition would be dwarfed as compared to its C_2 companion. In the CL spectra described in Part 1, we have not measured such large differences between the radiances of these two peaks at current densities up to 5 mA/cm^2. The current densities in scanning electron microscopes are much larger than 5 mA/cm^2 as discussed[2] and if the kinetic energy of the electrons would completely be absorbed by the phosphor particles, these latter would evaporate. Fortunately, at 200 keV more than 99% of the beam energy passes the nanosized phosphor particles. If saturation would be the case, the ratio R_{p3}/R_{p6} must be large at small Tb^{3+} concentration and will decrease at larger concentrations. Since the opposite is observed, as shown in Figures 10 (CL-curve) and 11b, it can be concluded that saturation may be ruled out at beam energy of 200 keV. From the CL spectrum of 0.7% Y_2O_3:Tb^{3+} represented in Figure 3, which was recorded at 80 keV, it can be seen that the ratio R_{p3}/R_{p6} differs substantially from the value for 0.7% Y_2O_3:Tb^{3+} as represented in Figure 11b. At this condition we cannot rule out saturation. The penetration depth at electron energy of 80 keV is still much larger than the phosphor particle size; however, the time of contact between beam electrons and lattice ions is longer than at 200 keV, which enables stronger interaction and more energy transfer from the E-beam to the phosphor. From the foregoing reasoning it can be concluded as a side note that current density does not seem the obvious criterion for studying phosphor saturation in a scanning electron microscope: other properties of the E-beam need to be considered to enable quantitative analyses.

Besides saturation there is another mechanism that might explain the odd ratio R_{p3}/R_{p6} in the CL spectrum depicted in Figure 3, viz. energy transfer from a Tb^{3+} ion at a C_{3i} site to Tb^{3+} at a C_2 site. In the previous section it has been assumed that the temperatures of the phosphor particles and holder are identical; however, at high energy transfer from E-beam to phosphor target this assumption is not particularly likely. If at 80 keV more energy from the E-beam is transferred to the phosphor particles than at 200 keV, the phosphor particles may be heated and according to the Arrhenius plot shown in Figure 12 this would result in more energy transfer from C_{3i} to C_2. From the measured ratios R_{p3}/R_{p6} for 0.7% Y_2O_3:Tb^{3+} at 80 keV and 200 keV the temperature in the phosphor particles bombarded with 80 keV electrons can be calculated from the average activation energy of 0.007 eV. The phosphor temperature would be between −30 °C and −10 °C: much higher than the holder, which is at −170 °C. From our results it cannot be concluded which mechanism is most likely: saturation or energy transfer from C_{3i} to C_2. It is probable that both mechanisms play a role.

For comparison reasons we present in Figure 14 the excitation spectra of cubic nanosized Y_2O_3:Eu^{3+} monitored at 611 nm and 582 nm: the transition at 611 nm has C_2 symmetry, while the weak transition at 582 nm has C_{3i} symmetry.[2] It can be seen that the C_2
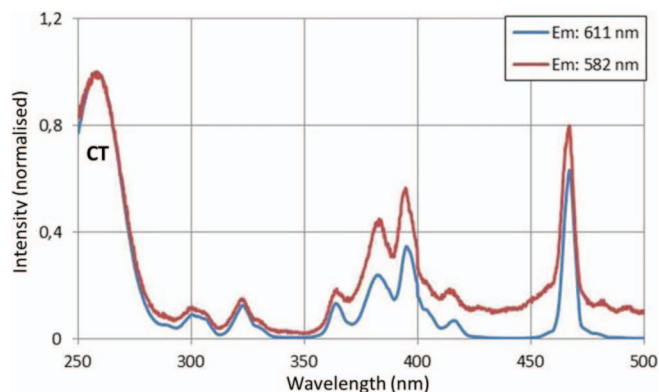
Figure 14. Excitation spectra of nanosized cubic 1% Y_2O_3:Eu^{3+} at 25° C monitored at 611 nm (C_2) and 582 nm (C_{3i}). Spectra have been normalized at 260 nm.

and C_{3i} CT-bands of Y_2O_3:Eu^{3+} at about 260 nm are equal. The back ground level in the C_{3i} -type spectrum recorded at 582 nm is higher, because this transition is much weaker than the 611 nm transition. Unlike Figure 4, which refers to Y_2O_3:Tb^{3+}, Figure 14 shows that it is impossible to excite symmetry-related energy levels in Y_2O_3:Eu^{3+} by irradiation with UV light at wavelengths between 250 nm and 300 nm.

Conclusions

The PL and CL spectra of cubic nanosized Y_2O_3:Tb^{3+} show differences as a function of Tb^{3+} concentration and temperature. We have interpreted these differences in terms of symmetry-related effects: viz. Tb^{3+} at C_2 and C_{3i} lattice sites of cubic Y_2O_3. From our analyses it can be concluded that at high Tb^{3+} concentrations and temperatures higher than 100 K, excitation energy will be transferred via radiation-less processes from Tb^{3+} at C_{3i} lattice sites to Tb^{3+} at C_2 lattice sites. This energy transfer occurs from the $^5D_4$ (C_{3i}) to the $^5D_4$ (C_2) level.

Perhaps surprisingly for such a well-known phosphor, we did not find symmetry-related analyses of the CL and PL spectra of Y_2O_3:Tb^{3+} in the literature.

References

1. D. den Engelsen, P. G. Harris, T. G. Ireland, G. Fern, and J. Silver, *ECS J. Solid State Sci. Technol.*, **4**, R105 (2015).
2. D. den Engelsen, P. G. Harris, T. G. Ireland, and J. Silver, *ECS J. Solid State Sci. Technol.*, **4**, R1 (2015).
3. H. Song and J. Wang, *J. Lumin.*, **118**, 220 (2006).
4. H. Najafov, Y. Satoh, S. Ohshio, A. Kato, and H. Saitoh, *Jpn. J. Appl. Phys.*, **43**, 7111 (2004).
5. R. E. Muenchausen, L. G. Jacobsohn, B. L. Bennett, E. A. McKigney, J. F. Smith, J. A. Valdez, and D. W. Cooke, *J. Lumin.*, **126**, 838 (2007).
6. L. Wang, N. Liao, L. Shi, H. Jia, P. Du, Z. Xi, and D. Jin, *Electrochem. Solid State Lett.*, **13**, E7 (2010).
7. T. Kano in *Phosphor Handbook*, 2nd ed., W. Yen, S. Shionoya, and H. Yamamoto eds., p. 197, CRC Press, Boca Raton (2007).
8. R. C. Ropp, *J. Electrochem. Soc.*, **111**, 311 (1964).
9. Q. Meng, B. Chen, W. Xu, Y. Yang, X. Zhao, W. Di, S. Lu, X. Wang, J. Sun, L. Cheng, T. Yu, and Y. Peng, *J. Appl. Phys.*, **102**, 093505 (2007).
10. Z. Liu, L. Yu, Q. Wang, Y. Tao, and H. Yang, *J. Lumin.*, **131**, 12 (2011).
11. S. Ray, A. Patra, and P. Pramanik, *Opt. Mater.*, **30**, 608 (2007).
12. R. S. Loitongbam, W. R. Singh, G. Phaomei, and N. S. Singh, *J. Lumin.*, **140**, 95 (2013).
13. S. Som, S. Dutta, Vijay Kumar, Vinod Kumar, H. C. Swart, and S. K. Sharma, *J. Lumin.*, **146**, 162 (2014).
14. A. Dobrowolska, E. C. Karsu, A. J. J. Bos, and P. Dorenbos, *J. Lumin.*, **160**, 321 (2015).
15. R. Withnall, M. I. Martinez-Rubio, G. R. Fern, T. G. Ireland, and J. Silver, *J. Opt. A: Pure Appl. Opt.*, **5**, S81 (2003).
16. M. E. Witkowski and A. J. Wojtowicz, *Optical Mater*, **33**, 1535 (2011).
17. A. Bril and F. A. Kröger, *Philips Tech. Rev.*, **12**, 120 (1950).